Analyses of representative elementary volume for coal using X-ray μ-CT and FIB-SEM and its application in permeability predication model

Hao Wu [a, b], Yanbin Yao [a, c*], Yingfang Zhou [d], Feng Qiu [a, b]

[a] School of Energy resource, China university of Geosciences, Beijing 100083, China

[b] Beijing Key Laboratory of Unconventional Natural Gas Geology Evaluation and Development Engineering University of Geosciences, Beijing 100083, China

[c] Coal Reservoir Laboratory of National Engineering Research Centre of CBM Development & Utilization, China University of Geosciences, Beijing 100083, China

[d] School of Engineering, University of Aberdeen, Aberdeen, AB243UE, United Kingdom

Abstract

The representative elemental volume (REV) study provides a bridge between macro and micro properties' research, which is critical for understanding and predicting the heterogeneous properties of a porous media. Permeability, one of the essential properties, dominates the capability of fluid flow in porous media, which is scale dependent and thus one of the most rationale way to predict macro scale permeability is to calculate the permeability at REV. Porosity is the most common parameter to determine REV, however, the porosity based REV works less satisfactory for complex pore system. In this work, we determined the REV based on fractal dimension, which is a fundamental parameter to characterize the complex pore network, and then the relation between fractal dimension and sample size was investigated extensively. We then determined and compared the REV from the porosity and fractal dimension that calculated from various sample sizes. Our results reveal that the relationship between fractal dimension-based REV and porosity-based REV can be classified as four cases, and the most common case is porosity declines if the domain is larger than fractal dimension-based REV size. The relation discussed above can be applied to existing fractal permeability models to predict the permeability at different scales.

Key words

Coalbed methane, 3D Pore structure, REV, Fractal dimension, Permeability

1 Introduction

Multiscale modelling is a common approach to predict the macro properties of porous media, such as sandstones, shales and coals. In some cases, the macro properties can be well characterized by micro scale study, and the minimum size of the sample that can be utilized to represent the macro scale sample is termed as REV, which was proposed by Bear [1] and the schematic was given as Fig. 1. As shown in this figure, the erratic fluctuations in region I reduce with the increasing sample size. In region II, the fluctuation becomes insignificant, which means the certain property of the sample becomes a constant that is not affected by sample size. Therefore, the left-hand side boundary of region II is taken as REV, for some physical properties of some porous mediums, the property values may change again as the sample size increases (region III in Fig. 1).

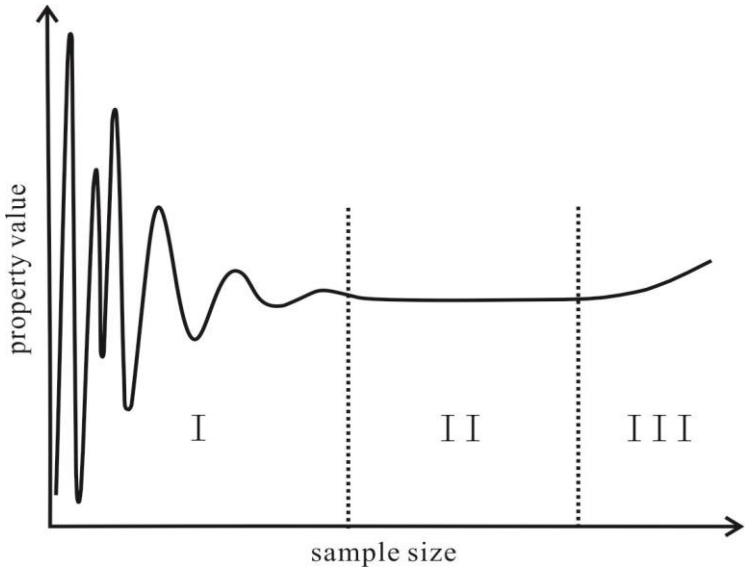

Fig. 1. Schematic of how REV is determined for a special property (modified from [1])

REV for different materials, such as reservoir rocks, including sandstones, siltstones, shales and limestones [2-4], soil [5,6] and cementitious materials [7], have been studied extensively. The most commonly used parameter to characterize REV is porosity [3,8], while other parameters, includes water saturation [9], tortuosity [6], Euler connectivity, average pore and throat volumes [7] have also been proposed to determine REV. However, the fractal dimension, one of the key parameters that describes complex pore system, has been rarely used to analyse REV for reservoir rocks.

Fractal theory was proposed by Mandelbrot [10], which gives a function to describe the relation between pore size and the cumulative number of pores. Since then fractal theory have been widely used to characterize the pore size distribution of reservoir rocks [11-13]. As for the calculation of fractal dimension, box counting method is one of the most effective methods to get fractal dimension value [14]. Box counting method is based on high resolution images, the fractal dimension that calculated using this method represents the fractal dimension of pore size and spatial distribution. Besides the image-based approach, fractal dimension could also be evaluated from different experiment measurements, such as volumetric fractal dimension by mercury intrusion experiment, surface and volumetric roughness fractal dimension from N_2 adsorption experiment and pore size distribution fractal dimension from NMR experiments. Furthermore, fractal theory has been widely used to characterize pore structures and seepage phenomenon in porous media, such as tortuosity, permeability and imbibition [15-18]. It is noticed that fractal theory is a powerful tool to better understand the complex pore structure and seepage procedures in porous media [19].

The recent advanced high-resolution imaging techniques (e.g. FIB-SEM, and X-ray micro-CT) make it easier and more effective to study the micro structure of porous media. Unlike conventional experiments such as mercury intrusion, both CT and FIB-SEM are non-destructive for pore structures characterization of reservoir rocks, especially in coal, whose pore structure is easy to be deformed [20]. Micro and mesoporous pore systems in coal that can be detected by μ-CT and FIB-SEM tomography are primary for gas adsorption [21], and the high resolution (2.5 nm for FIB-SEM and 1.1μm for CT in this work) of these techniques helps to extract the pore structure more accurately. These two different techniques with different resolutions make it possible to study and compare the multi-scale properties

of coal, like porosity, 3-D pore-throat characteristics and its connectivity [21, 22]. This helps to compare with and develop the numerical simulation of physical properties of reservoir rocks, which has been intensively developed in last few years [23]. These simulations are mainly performed in the micro tomography images of reservoirs rocks, so it is important to use high resolution techniques to characterize pore structure of reservoir rocks. However, as discussed above, REV has not been studied intensively using fractal dimension method based on high resolution images.

Coal is normally considered as a dual porosity media, including matrix and cleat system, in which the matrix is the main storage place for gas and cleats are the main pathway for gas flow. Recently, some researchers investigated the permeability model for fractured porous media based on fractal theory [24-27]. According to Miao et al. [24], properties like fractal dimension, porosity, maximum fracture length, maximum pore diameter in matrix, are the main parameters that determines the permeability. However, fractal dimension and sample size, porosity and sample size are normally related. According to the theory proposed by Yu et al. [28] and Yu et al. [29], the relation between porosity and fractal dimension can be characterized using a mathematic equation for fractal objectives. Based on the fractal permeability model proposed by Miao et al. [24], a novel model that can be used to predict permeability was obtained by combining the relation between fractal dimension REV and porosity REV. Some works have been done on predicting field scale permeability of shale [30,31], while in this work, we predicted the permeability at micro scale using high resolution coal images.

In this work, FIB-SEM and μ-CT scanner were utilized to accurately calculate the micro properties of anthracite coal samples. The images were processed, including denoise and binarization, and then the fractal dimension and porosity of these pre-processed images were estimated. The relation between fractal dimension-based REV and porosity REV were also discussed extensively. Finally, the relation between porosity and fractal dimension REV was applied to predict the permeability at different scales using the improved mathematic model.

2 Materials and Methods

2.1 Samples and coal analyses

Three different coal samples (DS, HC and YA) used in this study for X-ray μ-CT experiment were collected from Qinshui Basin, China, the maximum vitrinite reflectance are 2.92%, 4.06% and 4.69%, respectively, which means they are all anthracite in general. The sample AC was for FIB-SEM imaging, collected from Yangquan mine in Qinshui Basin, China, whose maximum vitrinite reflectance is 2.61%. The maximum vitrinite reflectance, maceral composition analyses followed the standards GB/T 6948-2008 and GB/T 8899-2013. The Automatic Proximate Analyzer 5E-6600 was utilized to complete the coal proximate analyses. Table 1 shows the results of the maximum vitrinite reflectance, coal maceral composition and coal proximate analyses of these samples.

Table 1. Vitrinite reflectance, maceral composition and proximate analysis of the coal samples

Sample NO.	R_o (%)	Coal maceral composition (vol. %)	Coal Proximate analysis (%)

		Vitrinite	Inertinite	Exinite	M_{ad}	A_d	C_{daf}
AC	2.61	83.55	12.15	0.0	1.20	13.30	73.01
DS	2.92	66.10	0.20	0.0	0.93	34.02	84.55
HC	4.06	63.80	31.70	0.0	1.03	9.33	83.35
YA	4.69	76.20	19.00	0.0	0.76	12.22	81.01

2.2 μ-CT scanning

Three smaller coal samples were drilled from each of the three original block samples. In order to avoid the influence of water dissipation on the experimental results, these three coal pillars were sealed in wax. The X-ray μ-CT scanning experiments were then performed utilizing the GE Phoenix X-ray Nanotom Industrial CT Instrument, which consists of X-ray source system, detector system, mechanical turntable system and image processing system [13]. The samples were placed perpendicular to the sample couch, then several typical coal samples were utilized to do preliminary experiments, which aimed to find out the best settings to reduce noise. The detector resolution was set to 2048×2048 pixels, in total, 2010 grey slices with the resolution of 1.1 μm were obtained for each sample. As shown in Supplementary materials, micro cleat systems can be detected using such a technique.

2.3 FIB-SEM imaging

Before the FIB-SEM experiment, cuboidal shaped coal sample with a size of 0.5×1×1 cm^3 was polished using dry emery paper to make the surface flat, then the sample was polished further by argon ion. Subsequently, sample was inserted into FEI Helios Nano Lab 650 FIB-SEM Dual-Beam system for imaging after being dried by putting it into the oven at 65 °C for 12 hours, details of this procedure followed the work of Holzer et al. [32] and Munch et al. [33]. A series of SEM images of the coal sample AC were obtained with a high resolution of 2.5 nm, the acceleration voltage is 2 kV and the working distance is 4 mm. Different from CT images, nanopores can be clearly observed in SEM images, so the comparison of the results computed from CT images and FIB-SEM images represents the different pore systems in coal.

2.4 Image processing

In order to eliminate the impact of the background edges, the three CT samples were cropped into three smaller cubes with different sizes according to their respective effective areas (see Supplementary materials). The side lengths of DS, HC and YA are 900 voxels, 400 voxels and 400 voxels, respectively. Side length of AC is 700 voxels.

Then each of these samples were cropped into different smaller cubes from nine different positions (A-I in Fig. 2A), and these smaller cubes can be regarded as ROI (selected region of interest in the image). The subvolume selection scheme that utilized in this work was proposed by Wu et al. [13], which can also be regarded as nine different grow regimes (self-similar regime) of a small cube to the original big cube (See Fig. 2). From each position, follow the certain direction, a new bigger cube was generated while the side length increases every 10 voxels until the side length reaches the original sample size (see Fig. 2B, which is an example from position I). Fox example, the side length of original

DS is 900 voxels, then 90 cubes will be generated for each selection scheme, side lengths of these small cubes range from 10 to 900, so there will be 802 (because nine cubes whose side lengths are 900 voxels are the same cube) different subvolumes.

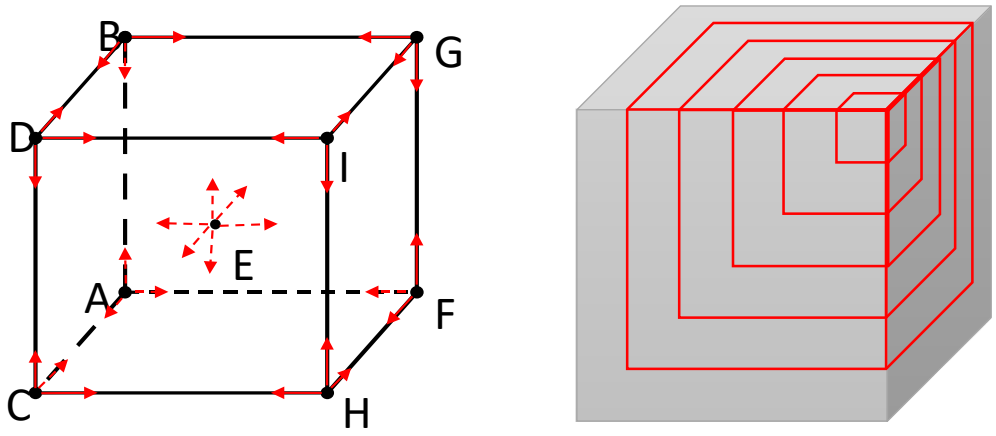

A *B*

Fig. 2. Subvolume (SV) selection schemes, A shows all nine schemes, B is an example of scheme I.

The raw grey images were processed with two main steps before being analysed. The first step is denoise, and it was applied to mitigate the noise in the original grey images using the median filter method with a radius equals to 2 voxels. The second step is binarization and segmentation. Coal is composed of three components, pores/fractures, coal matrix and minerals [34], each component has a special range of grey scale, and then these three parts can be separated by setting threshold values which are certain grey scale numbers. In this study, the threshold value was determined using Digital Terrain Model (DTM), which was proposed by Taud et al. [35]. Then the grey scale number of each pixel in the image was set to be 0 or 255 if the number is smaller or bigger than the threshold value, which is called binarization. The result of binarization is that image only contains black and white colour, which represent pores/fractures and other components, respectively.

2.5 Calculations

2.5.1 Calculation of porosity

Porosity of the porous media is given by

$$\varphi = \frac{V_p}{V_t} \qquad (1)$$

where φ is porosity, while V_p and V_t are the volume of pores and the volume of the sample, respectively. In this work, the porosity of these binarized images were determined by taking the ratio of the total voxels of void and the total voxels of the images and it was implemented in MATLAB.

2.5.2 Calculation of fractal dimension

According to the fractal theory proposed by Mandelbrot [10], numerous structures in the natural world, such as coastlines of the islands, shape of rivers and branches of a tree, are disordered and did not follow the Euclidean description, because their lengths, areas or volumes are not constants, but scale-dependent. The measure of a fractal structure can be done using box-counting method [13,14]

$$D_f = \lim_{r \to 0} \frac{\log(N_r)}{\log(\frac{1}{r})} \quad (2)$$

where, D_f is the 2D/3D fractal dimension, N_r is the number of boxes needed to cover the slices/cubes, r is the side length of the boxes.

3 Results and Discussion

3.1 Results of porosity-based REV and fractal dimension-based REV

Figs. 3-6 show REV analysis for fractal dimension of these coal samples. The x-axis represents the side length (voxels) of cubes, while y-axis represents fractal dimension of the 3D domain. As shown in these figure, erratic fluctuations in fractal dimension if the sample size is relatively small, this is consistent with the region I in Fig. 1. As the sample size increase, some lines begin to be steady (Fig. 1, region II). It can also be observed that different lines have different REV side lengths, this is due to the heterogeneity of coal. In this study, the biggest REV side length of these nine lines should be taken as the REV side length of the original sample. However, as shown in Figs. 3-6, some selection schemes (Figs. 4H, 4I, 5H) do not have REV, which means there is no REV for the original sample, so the REV discussed in this study is the REV for certain selection scheme. And this means that the fractal dimension REV can only be selected at certain positions for some coal samples. The smallest REV sizes of these 4 samples are 240 voxels, 320 voxels, 120 voxels and 90 voxels, respectively, while side lengths of these samples are 700 voxels, 900 voxels, 400 voxels and 400 voxels, respectively. Porosity REV of coal does not always exist (see Supplementary materials), which is inconsistent with the previous studies of sandstone, shale and other porous mediums [8,23,36]. However, REV exists for averaged porosity of these nine positions [13]. Another thing that can be observed from our experimental data is, for most schemes, porosity is not constant while fractal dimension already reaches REV, which shows trends that when fractal dimension reaches REV, porosity can also reach REV or increase or decrease.

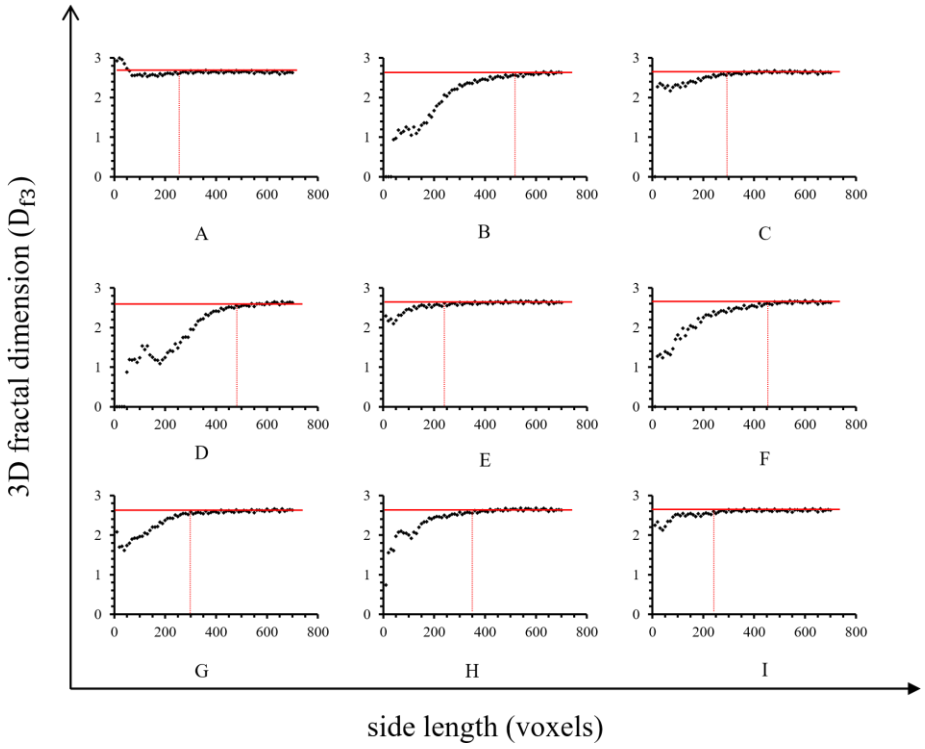

Fig.3. Fractal dimension stability with variation of cube length of AC, A-I represents different subvolume (SV) selection schemes (see Fig. 2)

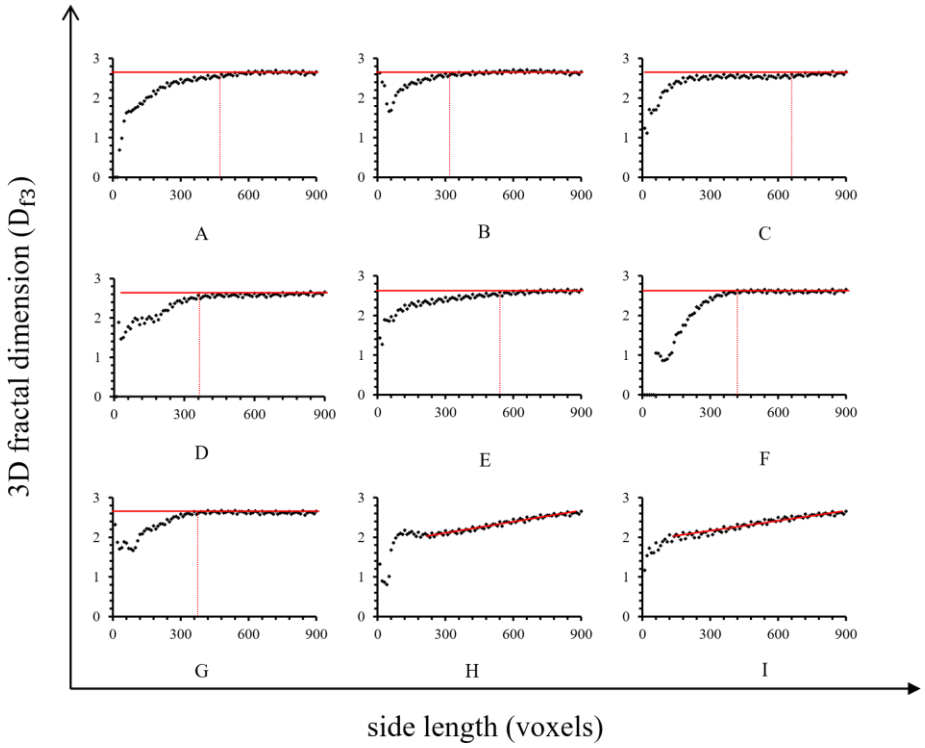

Fig. 4. Fractal dimension stability with variation of cube length of DS, A-I represents different subvolume (SV) selection schemes (see Fig. 2)

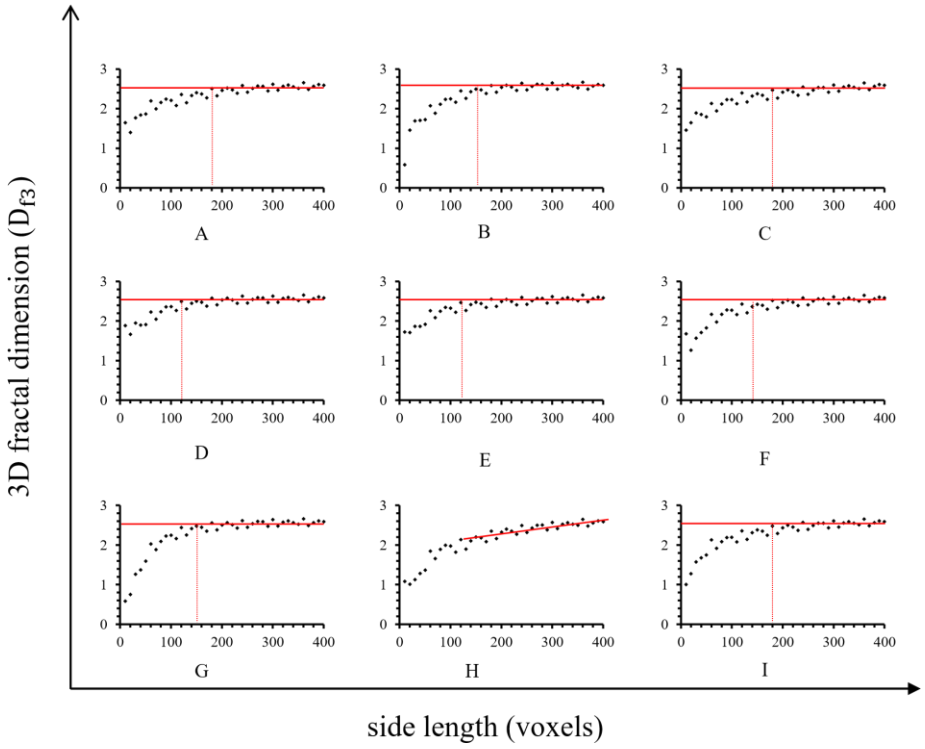

Fig. 5. Fractal dimension stability with variation of cube length of HC, A-I represents different subvolume (SV) selection schemes (see Fig. 2)

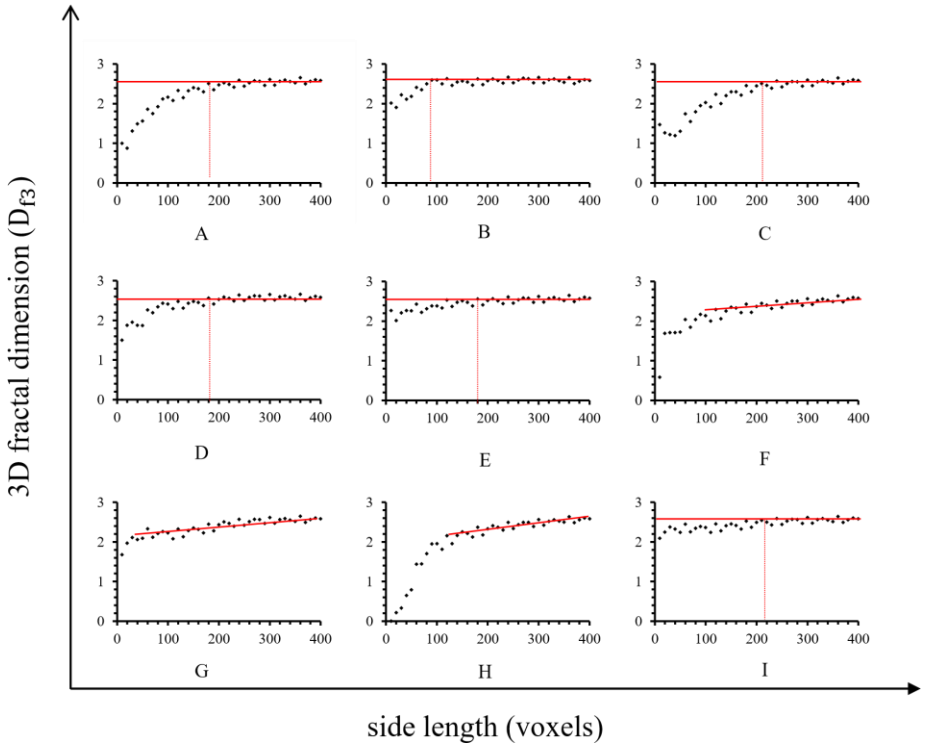

Fig. 6. Fractal dimension stability with variation of cube length of YA, A-I represents different subvolume (SV) selection schemes (see Fig. 2)

3.2 Discussion of porosity-based REV and fractal dimension-based REV

As shown above, the smallest fractal dimension REV side length of each sample relates to the size (voxel unit) of the sample and this relation is positive. This is because the bigger size of the sample, the

more data are needed to yield a value representative of the whole sample. The size here used is pixel/voxel unit, which is not the real size of these samples, for example side length of the smallest fractal dimension REV side length of AC is 240 voxels, and the resolution is 2.5 nm/voxel, which means that the actual side length is 0.6 μm. The side length of the smallest fractal dimension REV of YA is 90 voxels and the resolution is 1.1 μm, so the actual side length is 99 μm, which indicates that the size of REV is influenced by the resolution of the image: for images have similar size in voxel unit, the higher resolution, the smaller actual REV size. The fluctuation of fractal dimension REV and porosity REV values of each sample also indicates the heterogeneity of coal (Fig. 2). It is also noticed that REV exists only on some schemes, not all the schemes.

The relation between fractal dimension REV and porosity REV can be studied using fractal theory [28]. According to our experimental data, the relation between fractal dimension REV and porosity REV are concluded as four cases and they can be described using four examples:

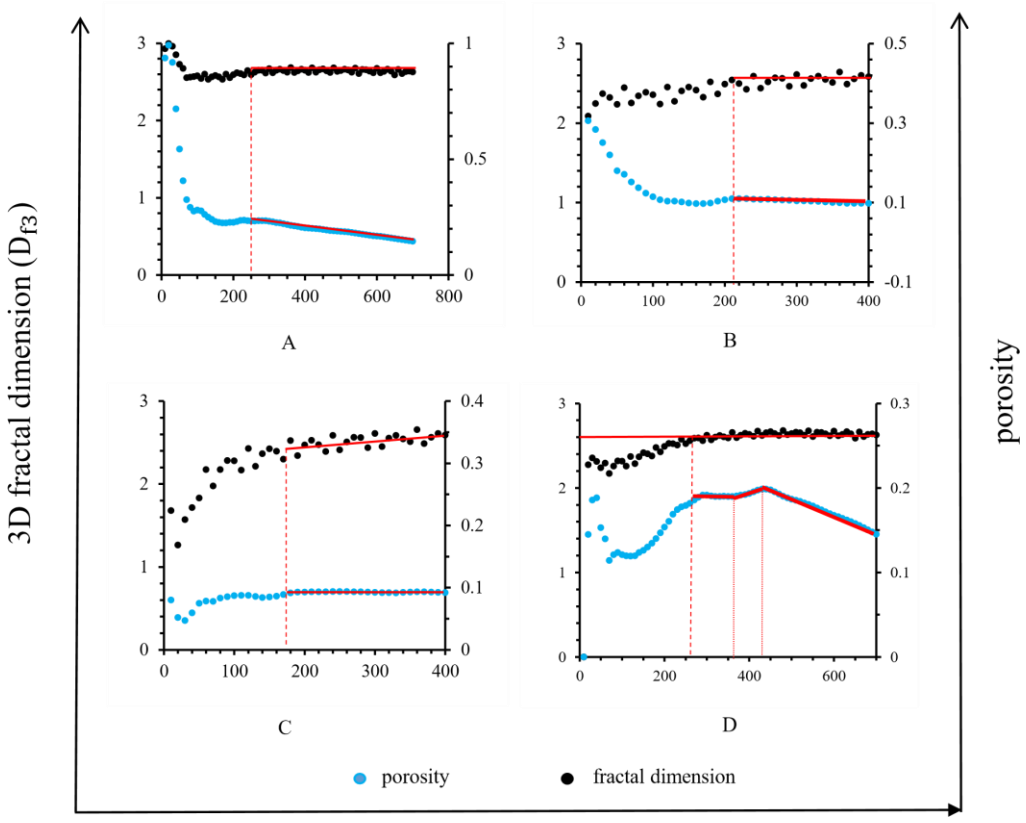

Fig. 7. A, B, C and D are porosity and fractal dimension stability with variation of cube length of scheme A of AC, scheme I of YA, scheme F of HC and scheme C of AC

These four examples can be concluded as four cases: Case 1: Fractal dimension reaches REV, while porosity declines (Fig. 7A); Case 2: Fractal dimension reaches REV, while porosity also reaches REV (Fig. 7B); Case 3: Fractal dimension increases, while porosity reaches REV (Fig. 7C); Case 4: Fractal dimension reaches REV, while porosity increases (Fig. 7D, which is combination of Case 1, 2, 4, and the middle part is Case 4).

Then all the schemes of these samples were counted (Table. 2) to find which case is the most common case for our coal samples, if a scheme contains more than one case, then count all of the cases.

The results show that Case 1 is the most common relation between fractal dimension REV and porosity for coal, which is porosity decreases when fractal dimension reaches REV.

Table2. Statistical results of the number of each case

	Case 1	Case 2	Case 3	Case 4	No REV
Number	25	4	5	6	6

3.3 Application in fractal permeability model

As discussed above, the relationship between fractal dimension REV and porosity REV can be categorised as four cases. When fractal dimension reaches REV, the relation between porosity and side length can be expressed as a mathematical correlation, and other parameters that used in the permeability model (Eq.3) could also described as a function of porosity, so that these parameters can be related to fractal dimension and side length. For example, the model proposed by Miao et al. [24] to analyse the permeability fractured porous media embedded with random fractures. In their model, permeability of fractal fracture network can be expressed as

$$K = \frac{\beta^3}{12A_f}\frac{D_{f,2D}\left(1-\cos^2\alpha\sin^2\theta\right)}{4-D_{f,2D}}l_{max}^4 \quad (3)$$

where D_f is the 2D fractal dimension of fractures, β is a proportionality coefficient, which is influenced by fracture toughness, Poison's ratio and Young's modulus [37], α and θ are the averaged fracture azimuth and the averaged fracture dip for fracture networks, respectively (Fig. 8). A_f is the cross-sectional area of a representative unit for fractal fracture networks, which is related to fractal dimension and porosity. l_{max} is the maximum fracture length, which is commonly related to the samples size positively [24]. If consider α, β and θ are constants, then permeability is influenced by D_f and l_{max}. As discussed above, when the model is used to predict permeability of different scales by changing sample size within a certain scale, just need to estimate the relation between D_f, l_{max}, φ and sample size. Then, because there exists REV for D_f, and l_{max} is commonly related to the samples size, so permeability can be related to sample size by then considering the relation between porosity and sample size. However, not all samples may have fractal dimension REV, and not all of their porosity values show decrease trend while fractal dimension reaches REV, what discussed in this part is the most common case. For example, for coal samples, Case 1 is mostly likely to happen, which means fractal dimension will be constant as the computation domain increase, while porosity will decrease, then according to the relation between porosity and cross-sectional area to estimate the change of the parameter cross-sectional area A_f.

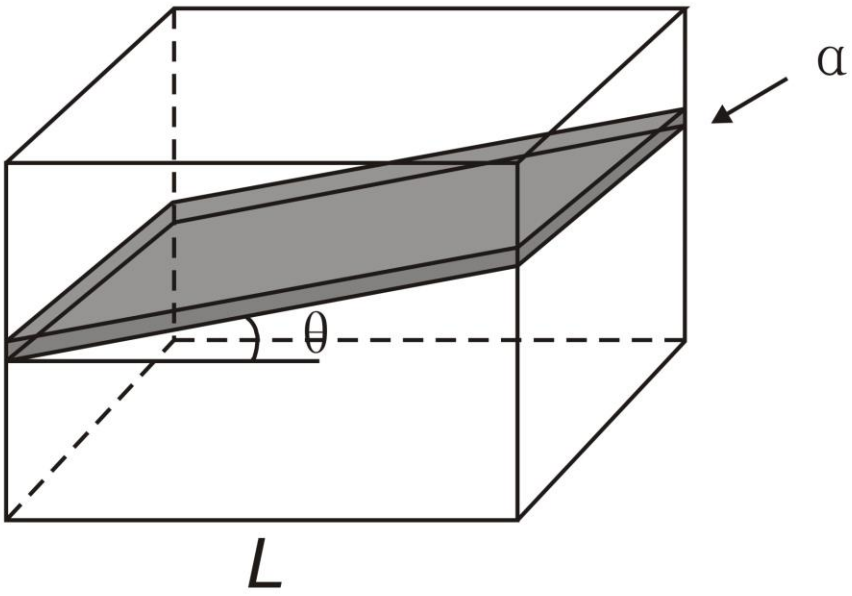

Fig.8 A single fracture in a representative structural unit, where α and θ are the fracture azimuth and the fracture dip, respectively, L is the sample length [24].

According to Miao et al. [24], cross-sectional area A_f can be expressed as

$$A_f = \frac{\beta D_{f,2D} l_{max}^2}{2-D_{f,2D}} \frac{1-\varphi}{\varphi} \quad (4)$$

where φ is porosity of fractures in the rock, D_f is the average two-dimension fractal dimension, which is approximately equal to three-dimension fractal dimension minus one [13].

Inserting Eq. (4) into Eq. (3) yields

$$K = \frac{\beta^2}{12} \frac{\varphi}{1-\varphi} \frac{(2-D_{f,2D})(1-\cos^2\alpha \sin^2\theta)}{4-D_{f,2D}} l_{max}^2 \quad (5)$$

The relation between porosity and side length can be estimated according to Case 1, which is a linear equation that can be obtained by adding a trend line, and then porosity is a function of side length of the sample,

$$\varphi = aL + b \quad (6)$$

where a and b are constants, L is side length.

The maximum fracture length is also a function of the side length, because the fractures in coal are straight (see Fig. 8), so the function can also be regarded as a linear equation as

$$l_{max} = \frac{L}{\cos\theta} \quad (7)$$

Inserting Eq. (6) and Eq. (7) into Eq. (5) yields

$$K = \frac{\beta^2}{12} \frac{aL+b}{1-aL-b} \frac{(2-D_{f,2D})(1-\cos^2\alpha\sin^2\theta)}{4-D_{f,2D}} \frac{L^2}{\cos^2\theta} \quad (8)$$

The only variable in Eq. (8) is side length *L*, so that Eq. (8) can be used to predict permeability of different scales. However, this equation is only applicable in certain scale ranges, as Eq. (6) only exists in a certain range of the sample side length. Eq. (8) was deduced based on the Case 1, which is the most common case, but other three equations can be deduced based on other three cases, which are uncommon.

In order to verify Eq. (8), the permeability of DS was simulated using LB (lattice Boltzmann) method, the simulation process was conducted through Palabos, which is an open non-commercial software that provides a framework for computational fluid dynamics. Then computation results can be visualized using Paraview, which is a powerful tool for visualization of scientific data (Fig. 9). As shown in Fig. 9, fracture is the main seepage pathway in coal. Fig.10 shows the results of LBM simulation.

Then pore network parameters needed in Eq. (8) were set according to sample DS scheme B: a is -0.0002, b is 0.3219, θ is 0° and $D_{f,2D}$ is 1.62. Side length was chosen from 600 to 900 voxels, which is because porosity decreases from 600 voxels. The data of these samples with side length from 600 to 850 were utilized to obtain β using Excel programming solver. Then this β value was utilized to calculate permeability of 900 voxels according to Eq. (8), after that, the error between computation result and simulation result was compared. Value of β using programming solver is 0.0018, and then the computation result for 900 voxels is 0.0062 μm^2, while the LBM result is 0.0063 μm^2, then the absolute error is 0.0001 μm^2, while the relative error is 1.6% (Fig.10).

However, the fractal dimension-based REV does not always exist, and porosity relates to side length linearly only within some range of the side length. Therefore, Eq. (6) is only applicable in some range of side length, so Eq. (8) is effective only within a certain range. Moreover, there may be some errors while conduct LBM permeability simulation, because the iteration is set as 60000 times. But 60000 times may not be big enough to ensure the simulation converge, even if the default value is only 30000 times for this simulation.

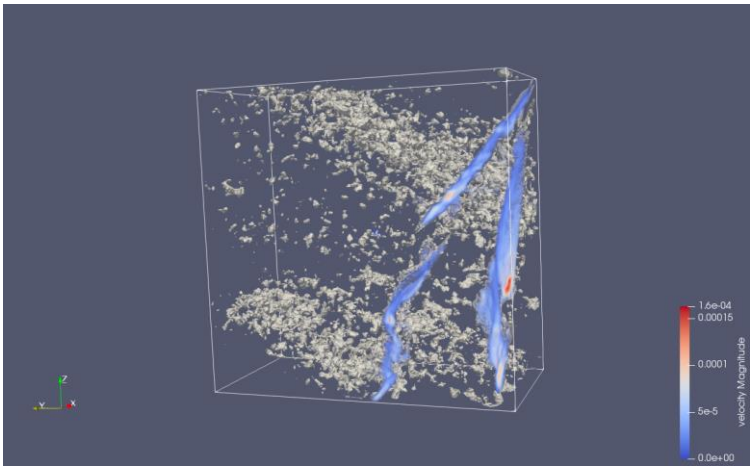

Fig.9 Fluid flow in the main fracture

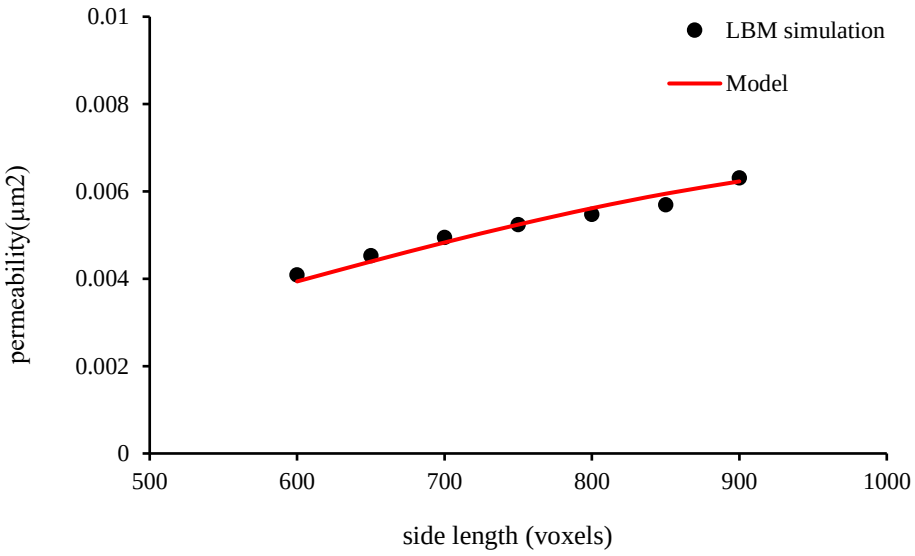

Fig. 10 Simulation results of sample permeability using LBM

4 Summary and Conclusions

In this work, high resolution μ-CT and FIB-SEM images of coal were utilized to obtain the accurate pore and fracture structure of coal, which were utilized further to analyse the porosity and fractal dimension of these samples. Based on the calculated results, the relation between fractal dimension REV and porosity REV was studied extensively. In conclusion, the main achievements presented in this work are:

(1) Fractal dimension-based REV does exist for coal, and the size (voxel unit) of the fractal dimension REV of each sample relates to the size (voxel unit) of the sample positively.

(2) For coal samples, REV should be selected at certain positions, even if the size of the REV is close to the original sample size.

(3) The relation between fractal dimension REV and porosity REV are concluded as four cases, while Case 1 is the most common relation in coal. And the relation can be applied to existing fractal permeability models to predict the permeability of different scales.

a) Case 1: Fractal dimension reaches REV, while porosity declines;

b) Case 2: Fractal dimension reaches REV, while porosity also reaches REV;

c) Case 3: Fractal dimension increases, while porosity reaches REV;

d) Case 4: Fractal dimension reaches REV, while porosity increases.

Future work of this study will be carried on other reservoir rocks (e.g. shale, sandstone and limestone) with the proposed approach in this study, then for different permeability models, try to characterise more parameters. More effort should be made to investigate the relation between maximum fracture length and sample size.

Acknowledgments

We acknowledge financial support from the National Natural Science Foundation of China (41872123; 41830427), the Petro China Innovation Foundation (2018D-5007-0101), the Key research and development project of Xinjiang Uygur Autonomous Region (2017B03019-1), the Royal Society Edinburgh through the international cost share scheme and National Natural Science Foundation China (NSFC 41711530129).

Reference

[1] Bear J. Dynamics of Fluids in Porous Media. American Elsevier Publishing Company, New York;1972.

[2] Fernandes JS, Appoloni CR, Fernandes CP. Determination of the Representative Elementary Volume for the Study of Sandstones and Siltstones by X-Ray Microtomography. Materials Research 2012; 15:662-670.

[3] Rozenbaum O, Du R, Rolland S. Representative elementary volume assessment of three-dimensional x-ray microtomography images of heterogeneous materials: Application to limestones. Physical Review E: Statistical, Nonlinear, and Soft Matter Physics 2014; 89:053304-053304.

[4] Adeleye JO, Akanji LT. Pore-scale analyses of heterogeneity and representative elementary volume for unconventional shale rocks using statistical tools. Journal of Petroleum Exploration and Production Technology 2018; 8:753-765.

[5] Li JH, Zhang LM, Wang Y, Fredlund DG. Permeability tensor and representative elementary volume of saturated cracked soil. Canadian Geotechnical Journal 2009; 46: 928-942.

[6] Borges JAR, Pires LF, Cássaro FAM, Roque WL, Heck RJ, Rosa JA, Wolf FG. X-ray microtomography analysis of representative elementary volume (REV) of soil morphological and geometrical properties. Soil & Tillage Research 2018;182: 112-122.

[7] Yio MHN, Wong HS, Buenfeld NR. Representative elementary volume (REV) of cementitious materials from three-dimensional pore structure analysis. Cement and Concrete Research 2017; 102: 187-202.

[8] Al-Raoush R, Papadopoulos A. Representative elementary volume analysis of porous media using X-ray computed tomography. Powder Technology 2010; 200: 69-77.

[9] Costanza-Robinson M, Estabrook B, Fouhey D. Representative elementary volume estimation for porosity, moisture saturation, and air-water interfacial areas in unsaturated porous media: Data quality implications. Water Resources Research 2011; 47(7).

[10] Mandelbrot B. The Fractal Geometry of Nature. W.H. Freeman, New York;1983.

[11] Katz AJ, Thompson AH. Fractal sandstone pores: implication for conductivity and pore formation. Phys. Rev. Lett. 1985; 54:1325–1328.

[12] Yao YB, Liu DM, Tang DZ, Tang SH, Huang WH. Fractal characterization of adsorption-pores of coals from north China: an investigation on CH4 adsorption capacity of coals. International Journal of Coal Geology 2008; 73:27–42.

[13] Wu H, Zhou YF, Yao YB, Wu KJ. Imaged based fractal characterization of micro-fracture structure in coal. Fuel 2019; 239: 53-62.

[14] Ai T, Zhang R, Zhou H, Pei J. Box-counting methods to directly estimate the fractal dimension of a rock surface. Applied Surface Science 2014; 314:610-621.

[15] Yu BM, Li JH. A Geometry Model for Tortuosity of Flow Path in Porous Media. Chinese Physics Letters 2004; 21: 1569-1571.

[16] Yao YB, Liu DM, Tang DZ, Tang SH, Huang WH, Liu ZH. Fractal characterization of seepage-pores of coals from China: an investigation on permeability of coals. Computer Geoscience 2009; 35:1159–66.

[17] Cai JC, Hu XY, Standnes DC, You LJ. An analytical model for spontaneous imbibition in fractal porous media including gravity. Colloids and surfaces A: Physicochemical and Engineering Aspects 2012; 414: 228-233.

[18] Zheng SJ, Yao YB, Liu DM, Cai YD, Liu Y, Li XW. Nuclear magnetic resonance T2 cut offs of coals: A novel method by multifractal analysis theory. Fuel 2019; 241: 715-724.

[19] Cai JC, Hu XY, Xiao BQ, Zhou YF, Wei W. Recent developments on fractal-based approaches to nanofluids and nanoparticle aggregation. International Journal of Heat and Mass Transfer 2017; 105: 623-637.

[20] Yao YB, Liu DM. Comparison of low-field NMR and mercury intrusion porosimetry in characterizing pore size distributions of coals. Fuel 2012; 95: 152-158.

[21] Li Z, Liu D, Cai Y, Ranjith P, Yao Y. Multi-scale quantitative characterization of 3-D pore-fracture networks in bituminous and anthracite coals using FIB-SEM tomography and X-ray μ-CT. Fuel 2017; 209: 43-53.

[22] Liu SQ, Sang SX, Wang G, Ma JS, Wang X, Wang WF, Du Y, Wang T. FIB-SEM and X-ray CT characterization of interconnected pores in high-rank coal formed from regional metamorphism. Journal of Petroleum Science and Engineering 2017; 148: 21-31.

[23] Gonzalez JL, de Faria EL, Albuquerque MP, Albuquerque MP, Bom CR, Freitas JCC, Cremasco CW, Correia MD. Representative elementary volume for NMR simulations based on X-ray microtomography of sedimentary rock. Journal of Petroleum Science and Engineering 2018; 166: 906-912.

[24] Miao TJ, Yu BM, Duan YG, Fang QT. A fractal analysis of permeability for fractured rocks. International Journal of Heat and Mass Transfer 2015; 81: 75-80.

[25] Miao TJ, Yang SS, Long ZC, Yu BM. Fractal analysis of permeability of dual-porosity media embedded with random fractures. Int. J. Heat Mass Transfer 2015; 88:814-821.

[26] Miao, TJ, Chen AM, Xu Y, Cheng SJ, Wang KD. A Permeability model for water-gas phkase flow in fractal fracture networks. Fractals 2018; 26 (6): 1850087.

[27] Yang Y, Yang H, Tao L, Yao J. Microscopic Determination of Remaining Oil Distribution in Sandstones with Different Permeability Scales Using Computed Tomography Scanning. ASME. J. Energy Resour. Technol. 2019;141(9):092903-092903-11.

[28] Yu BM, Li JH. Some fractal characters of porous media. Fractals 2001; 9: 365-372.

[29] Yu BM, Liu W. Fractal Analysis of Permeabilities for Porous Media. AIChE Journal 2004: 50; 46-57.

[30] Singh H, Cai JC. A Feature-Based Stochastic Permeability of Shale: Part 1—Validation and Two-Phase Permeability in a Utica Shale Sample. Transport in Porous Media 2019; 126:527-560.

[31] Singh H, Cai JC. A Feature-Based Stochastic Permeability of Shale: Part 2–Predicting Field-Scale Permeability. Transport in Porous Media 2019; 126:561-578.

[32] Holzer L, Muench B, Wegmann M, Gasser P, Flatt RJ. FIB-Nano tomography of particulate systems-part I: particle shape and topology of interfaces. Journal of the American Ceramic Society 2006; 89: 2577–2585.

[33] Münch B, Gasser P, Holzer L, Flatt R. FIB-Nano tomography of particulate systems-part II: particle recognition and effect of boundary truncation. Journal of the American Ceramic Society 2006; 89: 2586–2595.

[34] Yao YB, Liu DM, Che Y, Tang SH and Huang WH. Non-destructive characterization of coal samples from China using microfocus X-ray computed tomography. International Journal of Coal Geology 2009; 80:113-123.

[35] Taud H, Martinez-Angels R, Parrot J, Hernandez-Escobedo L. Porosity estimation method by X-ray computed tomography. Journal of Petroleum Science and Engineering 2005; 47: 209–217.

[36] Müller C, Siegesmund S, Blum P. Evaluation of the representative elementary volume (REV) of a fractured geothermal sandstone reservoir. Environmental Earth Sciences 2010; 61: 1713-1724.

[37] Klimczak C, Schultz RA, Parashar R, Reeves DM. Cubic law with aperture length correlation: implications for network scale fluid flow. Hydrogeol. J. 2010; 18 (4): 851–862.

Appendix A. Supplementary materials

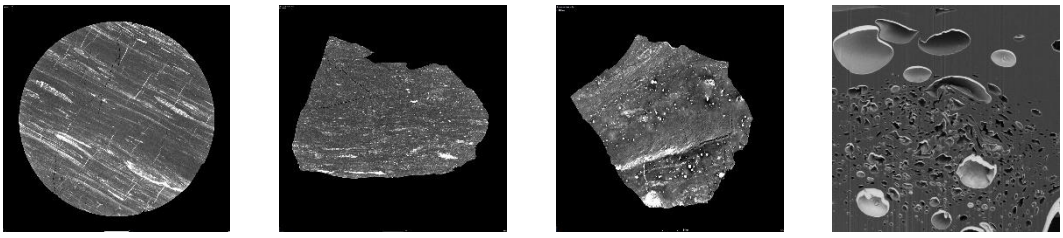

CT Slices (DS, HC and YA) and SEM image (AC) of coal samples

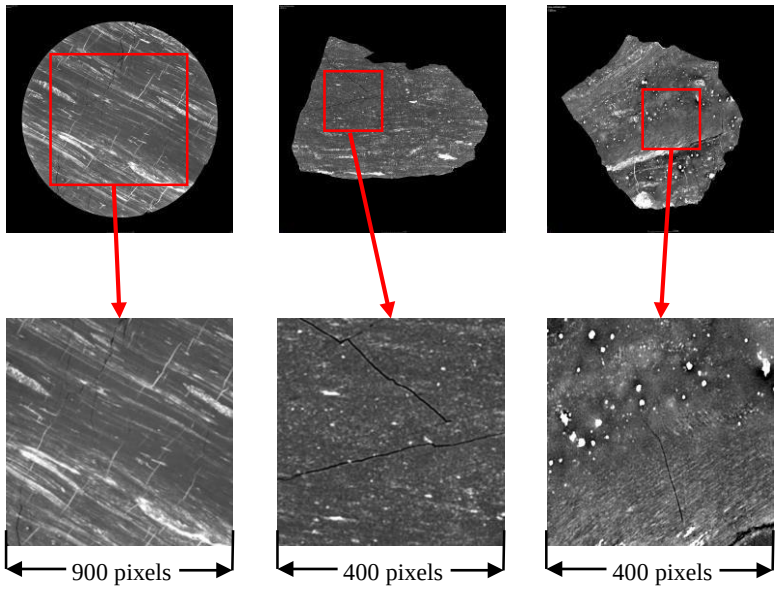

Selection of effective area in CT images

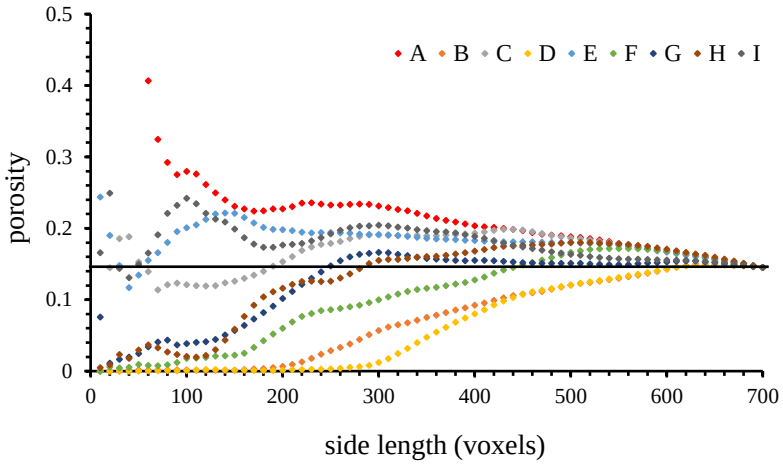

Porosity stability with variation of cube length of AC, A-I represents different subvolume (SV) selection schemes (see Fig. 2)

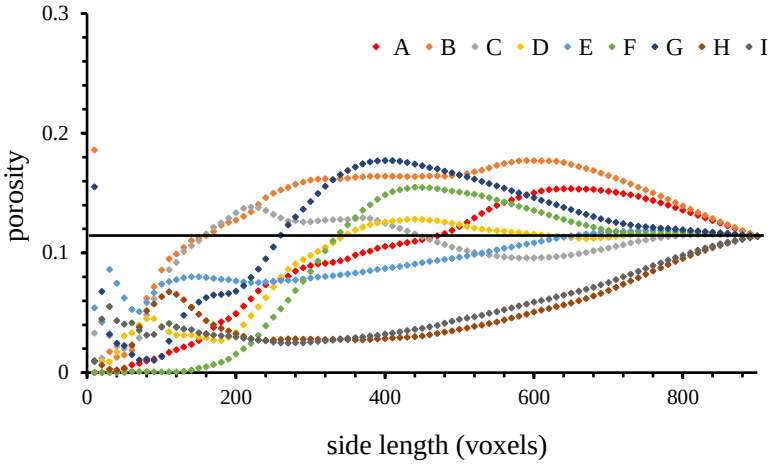

Porosity stability with variation of cube length of DS, A-I represents different subvolume (SV) selection schemes (see Fig. 2)

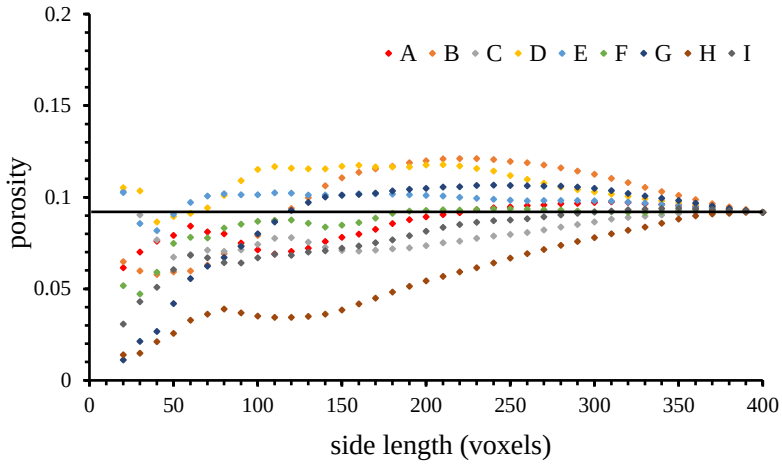

Porosity stability with variation of cube length of HC, A-I represents different subvolume (SV) selection schemes (see Fig. 2)

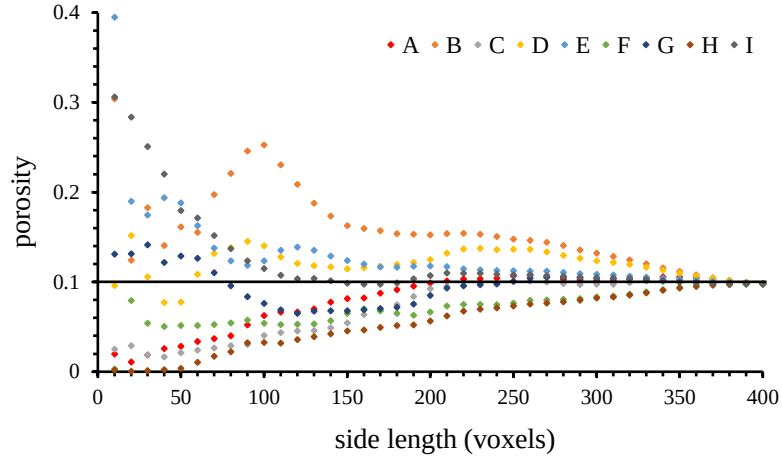

Porosity stability with variation of cube length of YA, A-I represents different subvolume (SV) selection schemes (see Fig. 2)